

# Performance of Swashplateless Helicopter Rotor with Trailing-Edge Flaps for Primary Flight Control



Jinwei Shen\*  
Senior Research Scientist  
National Institute of Aerospace  
Hampton, VA



Inderjit Chopra  
Alfred Gessow Professor  
University of Maryland  
College Park, MD



Wayne Johnson  
Aerospace Engineer  
NASA Ames Research Center  
Moffett Field, CA

A comprehensive analysis is developed to evaluate the rotor performance of plain trailing-edge flaps (TEF) as rotor primary control system. A parametric study is conducted to investigate the effects of various rotor and TEF design variables on rotor performance. The rotor studied is a two-bladed teetering rotor of an ultralight helicopter. The analytical model includes a teetering rotor formulation and a coupled trim procedure for determining TEF inputs. Computational fluid dynamics generated airfoil tables are used to obtain the TEF aerodynamic loads. A correlation study for the basic conventional rotor with primary pitch feather controls was performed using calculations from another comprehensive analysis. The results show good agreement for blade natural frequencies, rotor collective and cyclic pitch controls, and shaft tilt angles. Calculations of required TEF deflections and rotor power are carried out at different advance ratios for the swashplateless configuration. The results show the swashplateless configuration achieves better performance than the conventional rotor in forward flight, because of the reduction of parasite drag resulting from the elimination of the swashplate mechanical system. The optimal selection of blade pitch index angle, flap location, length, and chord ratio is aimed at reducing TEF deflections and rotor power.

## Nomenclature

$C_T$	rotor thrust coefficient
$c$	blade chord
$c_d$	section drag coefficient
$c_h$	section flap hinge moment coefficient
$c_l$	section lift coefficient
$c_m$	section pitching moment coefficient
$R$	rotor radius
$r_{mid}$	flap middle section spanwise location, nondimensional
$\alpha_s$	longitudinal rotor shaft tilt angle, positive nose down
$\beta_{1c}$	longitudinal rotor tip-path-plane tilt angle, positive forward
$\beta_{1s}$	lateral rotor tip-path-plane tilt angle, positive toward retreating side
$\delta$	trailing-edge flap deflection, positive trailing-edge down
$\delta_0$	trailing-edge flap collective angle
$\delta_{1c}$	trailing-edge flap lateral cyclic
$\delta_{1s}$	trailing-edge flap longitudinal cyclic
$\mu$	advance ratio
$\sigma$	rotor solidity
$\phi_s$	lateral rotor shaft tilt angle, positive advancing side down

$\psi$	azimuth angle
$\Omega_0$	nominal rotor rotational speed, 525 rpm
$\omega$	natural frequency of blade elastic mode

## Introduction

Trailing-edge flap (TEF) systems for primary flight control date back to the earliest days of rotorcraft development (Ref. 1). In recent years, the emergence of high-energy density smart material actuators has led to interest in TEF as a means for vibration and noise control as well as rotor performance enhancement (Refs. 2–4). The use of a TEF for primary flight control appears attractive in the context of an actively controlled rotor where embedded flaps can perform multiple functions.

A conventional helicopter mechanical control system typically consists of a swashplate, pitch links, pushrods, and hydraulic flight control actuators. This system contributes significantly to the weight, drag, and maintenance time of the aircraft and hence degrades the overall mission performance, reduces service life, and increases operating cost. Eliminating the swashplate assembly will result in a reduction in parasitic drag, maintenance cost, and, potentially, aircraft empty weight (Ref. 5).

Early studies by Lemnios and Wei and co-workers (Refs. 6–8) presented modeling and correlation of rotor performance for Kaman's SH-2 rotor, which utilizes a servo-flap type system as a primary control device. Straub and Charles (Ref. 9) examined the preliminary requirements of the swashplateless design for an Advanced Rotor and Control System

\*Corresponding author; email: shenjw@nianet.org.

Revised version of two papers presented at the American Helicopter Society 59th Annual Forum, Phoenix, AZ, May 6–8, 2003, and Heli-Japan 2002 Conference, Tochigi, Japan, November 11–13, 2002. Manuscript received January 2006; accepted June 2010.

(ARCS) concept. Phillips and Merkley examined the potential benefits of active control while eliminating the need for portions of the conventional helicopter flight control system with TEF (Ref. 10). A recent study by Ormiston, using a simple rigid rotor model, explored the feasibility of a swashplateless rotor with plain TEF (Ref. 11). This study concluded that the on-blade TEF system has the potential to satisfy general requirements for primary flight control and the profile power penalty associated with flap deflection may be acceptable with the use of pitch indexing (precollective). In a recent study, the authors developed a comprehensive analysis (Ref. 12) for a swashplateless rotor with TEF based on University of Maryland Advanced Rotorcraft Code (UMARC) (Ref. 13). The analysis was carried out on a five-bladed bearingless rotor system (modified MD 900 rotor) with a soft pitch link (fundamental blade torsional frequency of 2.1/rev). A multicyclic controller was implemented to minimize vibratory hub loads with the swashplateless rotor system. The plain flaps were shown to have the capability of performing both primary rotor control and active vibration control functions. In addition, the authors conducted a parametric study (Ref. 14) to identify the key parameters in the design of a swashplateless rotor with TEF.

The power penalty associated with the TEF deflection, an important issue with the swashplateless design, has not been systematically studied. The aerodynamic loads of the TEF airfoil, especially the drag, are very complicated and difficult to predict with lifting line theory. These loads must either be measured experimentally or calculated using computational fluid dynamics (CFD) to obtain accurate TEF aerodynamics for rotor performance analysis. The objective of the present study is to evaluate the performance of the plain TEF swashplateless rotor system by using CFD-generated airfoil aerodynamics tables. The paper also investigates the effect of various key design variables, namely pitch index angle, flap location, and flap size on rotor performance and TEF deflections and actuation requirements.

**Analytical Model**

The selected baseline helicopter for the swashplateless rotor configuration is an Ultraspot 496 built by American Sportscopter (ASI). The first flight of the 496 was completed in July 1995. ASI 496 utilizes a two-blade teetering rotor design and has an empty weight of 540 lb, a Hirth 95-hp engine, and a cruise speed of 61 kt ( $\mu = 0.16$ ). Rotor and vehicle properties are given in Table 1. An unmanned air vehicle (UAV) version of the ASI 496 was selected as an ultralight helicopter flight-test platform for the NASA Revolutionary Concepts (REVCON)

**Table 1. ASI 496 rotor and vehicle properties**

Rotor type	Teetering
Rotor rotation direction	Counterclockwise (viewed from above)
Number of blades	2
Rotor diameter	23 ft
Rotor speed	525 rpm
Chord	6.7 inches
Airfoil	VR-7
Linear twist angle	-8°
Lock number	5.01
Solidity	0.0309
Undersling	3.45 inches
Gross weight	912 lb
Design cruise speed	61 kt ( $\mu = 0.16$ )
Aircraft CG position (longitudinal)	0.75 inch forward of hub
Aircraft CG position (vertical)	50.6 inches below hub
Parasite drag area ratio	0.0315

**Table 2. Calculated normal mode frequencies for ASI 496 rotor single blade at rotating speed of 525 rpm**

Mode	Frequency (per rev)
First flap	1.11
First inplane	1.23
First torsion	2.20
Second flap	3.09
Third flap	5.78
Second inplane	7.42
Fourth flap	8.72

swashplateless flight project. The present study was undertaken in support of this program and was intended to evaluate the rotor performance and actuation requirements of a swashplateless ASI 496 rotor.

The baseline rotor analysis is adopted from UMARC (Refs. 13, 15). The present analysis incorporates a finite element methodology in space and time. In the analysis of the teetering rotor, it is important to treat both blades simultaneously because they are rigidly connected to each other and attached to the mast through a common teeter hinge. The blade equations of motion consist of the degrees of freedom of the two elastic blades and an additional degree of freedom of the teetering motion. The equations of motion are solved in the hub-fixed frame. The blade is modeled as an elastic beam undergoing flap bending, lag bending, elastic twist, and axial deformation. The rotor blades are discretized into a finite number of beam elements, each element with 15 degrees of freedom. Fifteen elements are used to model a single blade. The coupled blade response and the trim control settings are solved simultaneously for the propulsive trim condition. Eight time elements with fifth-order shape functions are used to calculate the coupled trim solution. The TEF motion is prescribed, and as such dynamics of the actuator is neglected for simplicity. (Ref. 16 investigated the actuator dynamics of TEF rotors.) UMARC predictions of the rotating blade frequencies in a vacuum with hub fixed are shown in Table 2. The conventional swashplate controlled system results in a rotating blade torsional frequency of 2.2/rev. The present swashplateless rotor design modifies the baseline rotor by replacing the pitch link assembly with a root spring. The torsional frequency of the swashplateless rotor is kept the same as that of the baseline rotor.

**Analysis of TEF rotor**

For a rotor with TEF for primary control, the flaps produce torsional moment changes that drive the main blades in pitch against the root spring to achieve aerodynamic equilibrium, thereby producing the desired collective and cyclic blade twist. The trim variables for a flapped rotor are flap collective deflection,  $\delta_0$ , and flap cyclic deflections,  $\delta_{1c}$  and  $\delta_{1s}$ .

To reduce actuation forces, the rotor must be torsionally soft, which can be achieved using soft root springs. To reduce the range of TEF deflections, the rotor blades need to be pitched with a nose-up preset angle that is higher than the collective pitch normally required to trim the helicopter. As the rotor is accelerated to its operating speed, the additional nose-down pitching moment generated by the flaps and inertia loads will pitch the blade nose-down to the desired pitch position. The precollective pitch is the blade pitch angle at 0.75R when the root spring is unloaded. This blade pitch index angle is an important design parameter that affects rotor performance and flap actuation requirements. For a nonindexed blade, the flaps need to be deflected to extremely large upward angles to twist the blade nose-up to achieve desired angles of attack. This in turn

results in an unfavorable reduction in lift that needs to be compensated. However, for a pitch-indexed blade, the flaps are only required to have a small deflection to obtain a desired torsional moment.

For a rotor with flaps for primary controls, the control angle input to a flap is given by

$$\delta(\psi) = \delta_0 + \delta_{1c}\cos(\psi) + \delta_{1s}\sin(\psi) \quad (1)$$

and the blade pitch angle consists of the blade index angle, blade built-in twist angle, blade elastic twist angle, and the pitch associated with deflection of the root spring. The flap control angles are calculated from the coupled trim procedure. This procedure solves the vehicle trim equations and the blade steady response equations. For propulsive trim in a steady flight condition, the trim solution is obtained by solving the three force (vertical, longitudinal, and lateral) and three moment (pitch, roll, and yaw) vehicle equilibrium equations. For a specified gross weight and flight speed, the trim solution calculates control angles, vehicle orientation (longitudinal and lateral shaft tilts), and tail rotor pitch. The control angles for a conventional rotor are collective pitch deflection ( $\theta_0$ ) and cyclic pitch deflections ( $\theta_{1c}$ ,  $\theta_{1s}$ ) while for flapped rotor they are collective flap ( $\delta_0$ ) and cyclic flap ( $\delta_{1c}$ ,  $\delta_{1s}$ ). The trim solution and blade responses are updated iteratively until the convergence criteria are satisfied. The incremental lift, drag, and pitching moments of the TEF, consisting of both inertial and aerodynamic contributions, are included in this coupled trim procedure.

The aerodynamic model of the present analysis uses a quasi-steady lifting line theory. The Drees linear inflow model is used to obtain the induced inflow distribution over the rotor disk. The aerodynamic coefficients are taken from C81-type airfoil tables. These airfoil lookup tables provide two-dimensional (2D) aerodynamic characteristics and contain the lift ( $c_l$ ), drag ( $c_d$ ), and pitching moment ( $c_m$ ) coefficients as functions of airfoil angle of attack and flow Mach number. For a TEF airfoil, the airfoil table has to be generated for different TEF angles. The aerodynamic characteristics are then a function of angle of attack, Mach number, and TEF deflection. Furthermore, an additional aerodynamic coefficient, flap hinge moment ( $c_h$ ) is included in the lookup table to calculate the TEF actuation moments.

These airfoil tables are generated using 2D OVERTURNS (Ref. 17), a CFD analysis. In view of the unavailability of TEF airfoil tables compiled with wind tunnel test data, CFD-generated tables are an appropriate alternative. 2D OVERTURNS is an overset structured mesh solver which solves the compressible RANS equations with the Spalart–Allmaras turbulence model. The grid used in this study is a  $329 \times 97$  C-grid. The Reynolds number is set to 4.8 million. The baseline ASI 496 airfoil is the Boeing VR-7. A TEF airfoil modifies the baseline VR-7 airfoil by replacing the trailing-edge part of the baseline airfoil with a movable flap. The flap hinge gap is assumed to be completely sealed.

## Results and Discussion

Initially, the present comprehensive analysis is validated for the baseline teetering rotor without TEF. Results from the present analysis are compared with calculations from CAMRAD II (Refs. 18, 19). The calculated results of blade natural frequencies in a vacuum, trim angles, blade flapping angle, and main rotor power are correlated. Following this, the predicted results of the rotor with embedded flaps are presented, and the effects of various important design variables are investigated.

### Baseline correlation

Figure 1 compares computed natural single blade frequencies from the present analysis with results obtained using CAMRAD II. Good

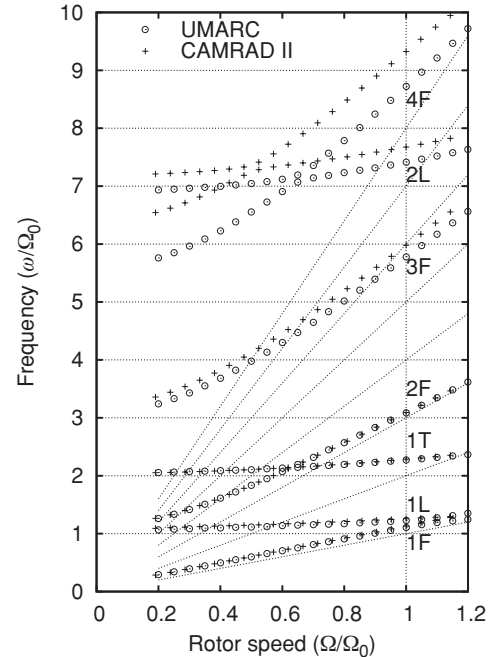


**Fig. 1. Comparisons of blade normal mode frequency for ASI 496 teetering main rotor.**

agreement is seen for the first and second flapwise bending modes, the first chordwise mode, and the first torsion mode. Some discrepancies exist in the fourth flapwise bending mode and second inplane mode predictions, possibly due to differences in modeling assumptions, to which these higher order coupled modes are particularly sensitive. Natural frequencies for the baseline rotor are summarized in Table 2 for the nominal rotating speed.

Figure 2 compares trim results and main shaft power for the baseline teetering rotor in level flight. Figure 2(a) shows the predicted values for blade collective pitch, longitudinal cyclic pitch, and lateral cyclic pitch for different advance ratios. Good agreement is seen between the two sets of results. Figure 2(b) shows the prediction of rotor shaft angles for different advance ratios. Good agreement is seen for the longitudinal shaft angles except at advance ratios greater than 0.1, where UMARC predicts slightly higher values. Lateral shaft tilt angles show the same trend. Slight discrepancies may be due to the different inflow models used by the two analyses (the present analysis uses Drees linear inflow, whereas the CAMRAD II model adopts a different nonuniform inflow model.) Figure 2(c) presents the calculated blade flapping angles (i.e., teetering angles). The UMARC longitudinal flapping angle results agree well with the CAMRAD II predictions. The lateral blade flapping angle shows some discrepancies between the two predictions. Figure 2(d) illustrates the computation of main rotor power for different advance ratios. Good agreement is seen for advance ratios above 0.15. For low advance ratios, UMARC predicts lower rotor power required than CAMRAD II. Again, the discrepancy may be a result of the differences in the inflow models used in the two analyses.

### Aerodynamics coefficients predicted by OVERTURNS

Figure 3 shows an example of the OVERTURNS calculations of the aerodynamic coefficients of the VR-7 TEF airfoil. Aerodynamic coefficients for three flap deflections, namely neutral, and 5 deg upward and downward, are shown as a function of angles of attack. Test data (Ref. 20) for the baseline airfoil (no TEF) are also included for comparison with

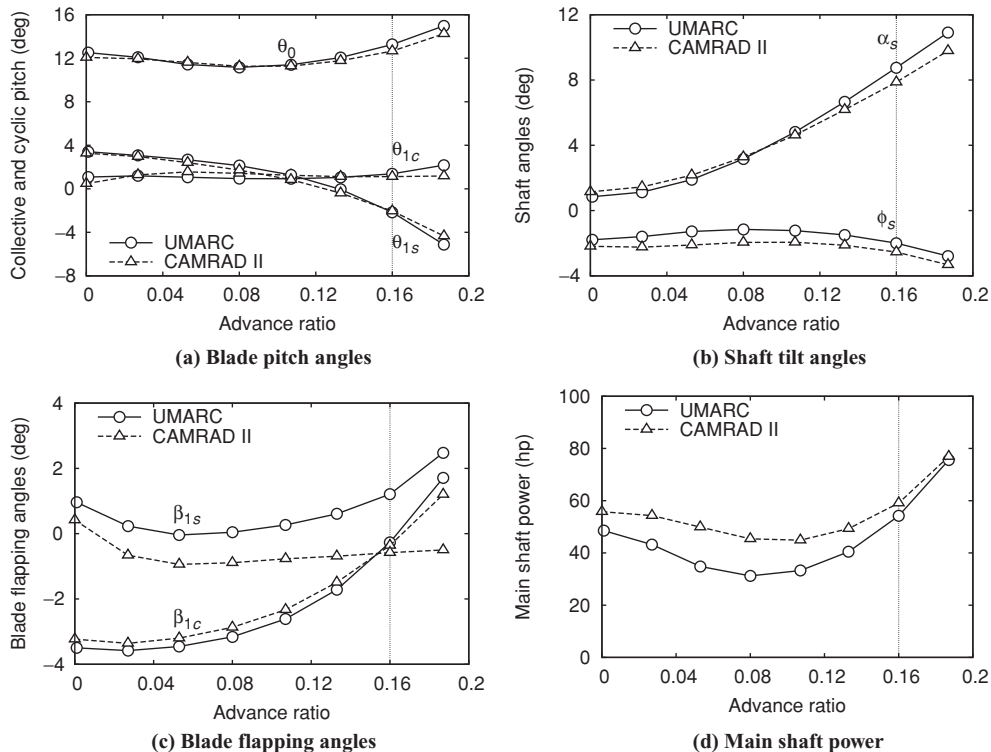


Fig. 2. Comparisons of blade pitch, shaft tilt, flapping angles, and main shaft power for the basic teetering rotor in level flight (nominal  $C_T/\sigma = 0.075$ ).

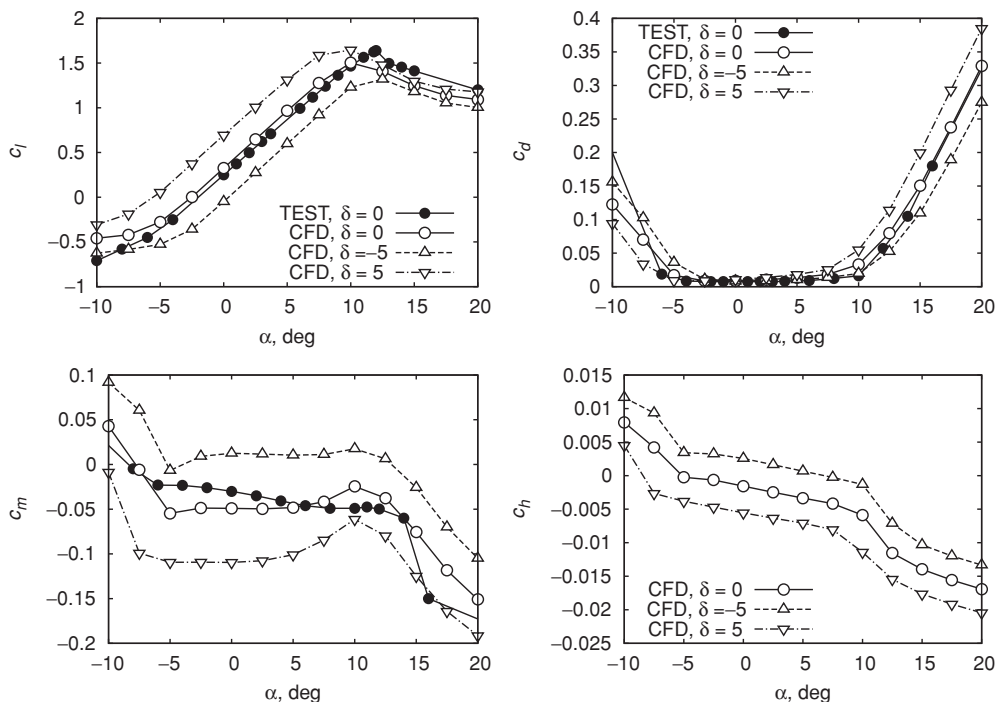
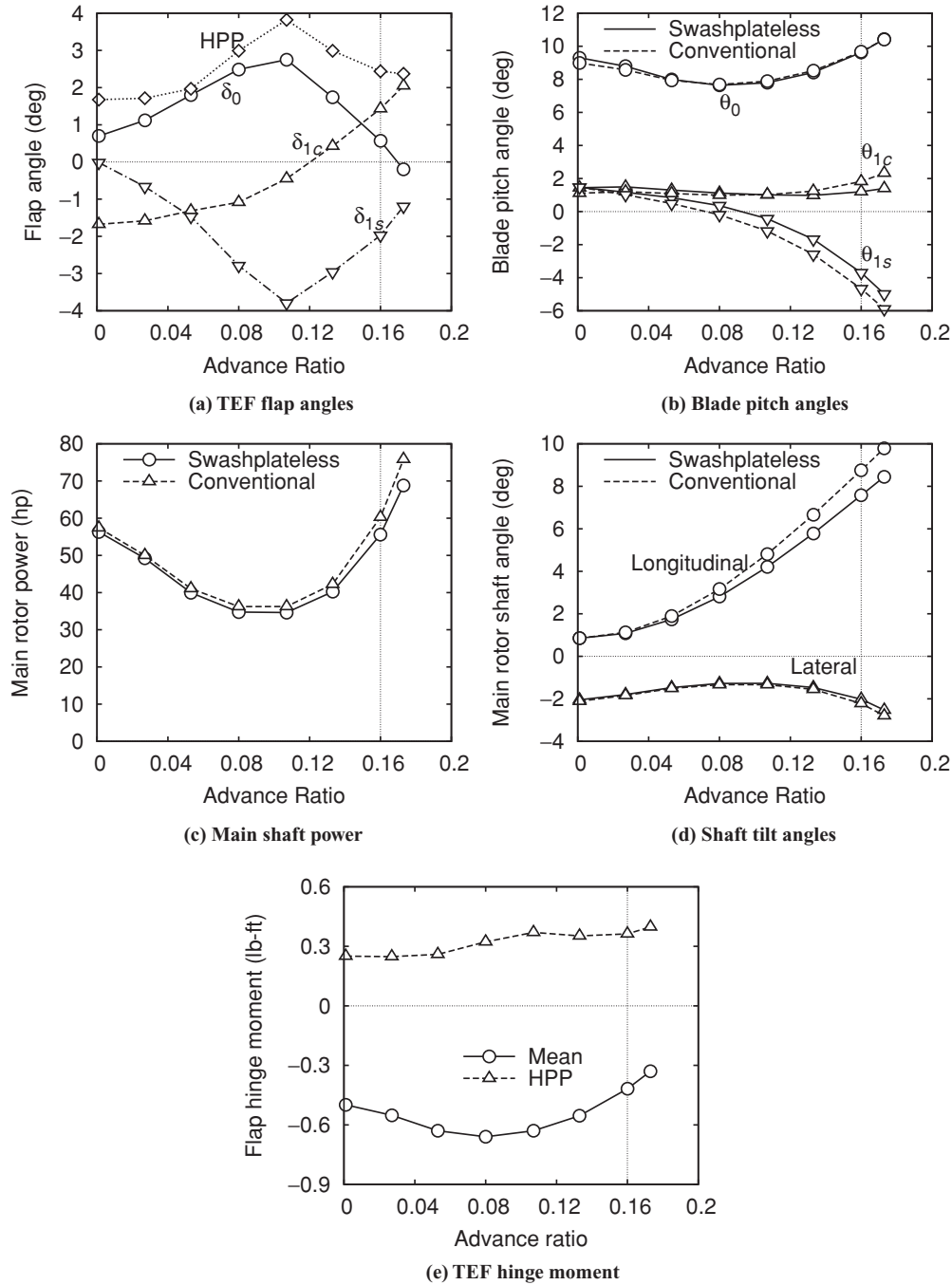


Fig. 3. Aerodynamic coefficients of TEF VR-7 airfoil (flap chord ratio = 0.25, Mach number = 0.5).

the neutral flap case as a means to validate the CFD calculations. Good agreement is seen for lift and drag coefficients. Calculated pitching moment coefficients also compare well with the test data but in a less degree than those of the lift and drag predictions. Sensitive to the airfoil pressure distribution, pitching moment is particularly difficult to compute consistently and accurately.

### Helicopter with baseline swashplateless rotor

The parasite drag area of ASI 496 helicopter with swashplateless configuration is selected at 85% of that of the conventional configuration in consideration of the elimination of the swashplate system. The 15% reduction in parasite drag area of the swashplateless configuration



**Fig. 4. Comparisons of conventional and swashplateless rotor at different forward speeds (nominal  $C_T/\sigma = 0.075$ ).**

is estimated on existing data of helicopter parasite drag. Reference 21 shows that the hub drag can contribute between 20% and 40% of the total helicopter drag. Although there is no specific drag data on the swashplate control system, it is known to be a large contributor in the total hub drag breakdown. In addition, this reduction is only selected to show the possible power saving by removing the swashplate system. The qualitative trend of the numerical simulations does not depend on the exact degree of reduction.

The baseline weight for both swashplateless and conventional configurations is 912 lb, which gives a  $C_T/\sigma$  of 0.075. The baseline TEF characteristics are given in Table 3. The TEFedge flap motion is positive for trailing-edge downward deflection, and hinge moment is positive when its direction is trailing-edge down.

**Table 3. ASI 496 rotor TEF properties**

Flap type	Plain flap
Spanwise length	25 inches (0.18R)
Chord ratio	25%
Flap midspan location	0.82R

Figure 4 compares conventional and swashplateless rotor control settings over the complete range of advance ratios ( $\mu = 0-0.17$ ). The swashplateless rotor has a pitch index angle of  $20^\circ$ , which yields small collective flap at the design cruise speed 61 kt ( $\mu = 0.16$ ).

Figure 4(a) presents the TEF deflection required to trim the swashplateless rotor. The required flap collective and cyclic angles are shown

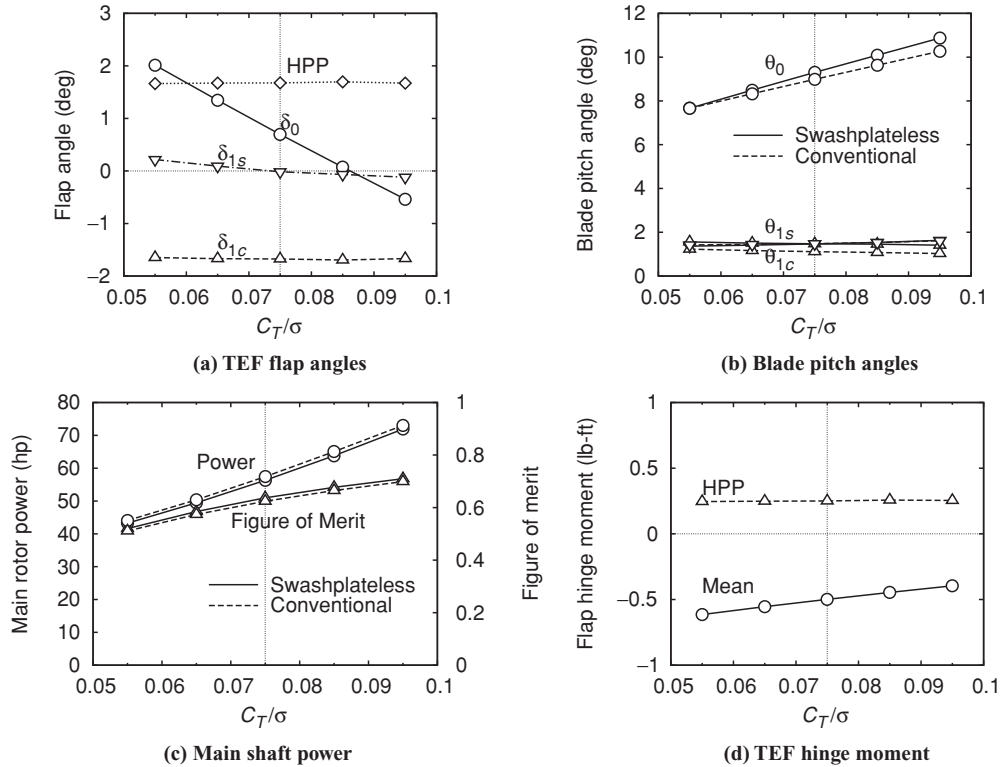


Fig. 5. Comparisons of conventional and swashplateless rotors for different thrust levels in hover.

to be below  $4^\circ$  over the complete range of advance ratios. The TEF collective angle,  $\delta_0$ , is deflected downward for the complete advance ratio range to pitch the blade nose down except at the highest speed. The half peak-to-peak (HPP) amplitude of flap motion, which is proportional to the actuation power required, is also below  $4^\circ$ .

Figure 4(b) compares the  $0.75R$  pitch angles of the conventional and swashplateless rotor. The pitch angle is relative to the hub plane, that is, the pitch index angle is included for the swashplateless rotor. In addition, the elastic blade twist angles, whose magnitude can be significant for the swashplateless configuration, are also included for both the conventional and swashplateless rotor shown in this and following figures (in contrast, the elastic twist is not included in Fig. 2(a)). As expected, blade pitch angles, both collective and cyclic, are shown to be similar for both configurations. The collective blade pitch of the swashplateless rotor is slightly greater than the conventional rotor in hover. The blade longitudinal and lateral cyclic pitches of the swashplateless rotor also show a small variation compared to the conventional rotor, because of the reduced parasite drag and the additional 1/rev lift variations due to the flap cyclic deflections,  $\delta_{1s}$  and  $\delta_{1c}$ .

Figure 4(c) compares main rotor power of the swashplateless and conventional rotors. In high-speed forward flight conditions, the swashplateless rotor consumes less power than the conventional rotor, again attributed to the assumed reduction of parasite drag. In hover and low-speed flight conditions, where parasite drag is less important, the swashplateless rotor requires slightly less power than the conventional rotor.

Figure 4(d) illustrates main rotor shaft angles for both configurations. The swashplateless rotor exhibits smaller forward tilt because of the reduction in parasite drag. The reduction is more significant as speed increases, diminishes at low speed, and becomes zero in hover. Lateral shaft tilt exhibits a slight difference between the two configurations.

Figure 4(e) shows the TEF hinge moments for different flight speeds. The mean values of the hinge moments are generally governed by the flap collective,  $\delta_0$ . The HPP value of the hinge moments shows an overall slight increase with airspeed, a result of the combined effects of the variation of flap cyclic and the increased aerodynamic unsteadiness with airspeed.

### Hover performance

Figure 5 evaluates the performance of swashplateless and conventional rotors in hover for different weight configurations. The ratio of thrust coefficient to rotor solidity,  $C_T/\sigma$ , varies from 0.055 to 0.095, corresponding to a gross weight range of 670–1155 lb.

Figure 5(a) shows that the flap collective decreases with higher  $C_T/\sigma$  because of the reduced blade pitch relative to the blade indexed pitch angle. Flap cyclic shows virtually no dependence on  $C_T/\sigma$  because the blade cyclic pitch are kept almost constant when  $C_T/\sigma$  changes.

Figure 5(b) compares the blade pitch of the swashplateless and conventional rotors. As expected, the blade collective pitch angles increase with  $C_T/\sigma$ , and the blade cyclic pitch angles are almost constant versus  $C_T/\sigma$  (cyclic pitch is applied to balance the tail rotor thrust and compensate for the aircraft CG offsets).

Figure 5(c) evaluates the performance of the swashplateless and conventional rotors by comparing the main shaft power and figure of merit. The swashplateless rotor consumes slightly less power than the conventional and has a slightly higher figure of merit in the range of  $C_T/\sigma$  considered. This phenomenon was also noted in Ref. 8.

Figure 5(d) presents the flap hinge moments. Mean hinge moments decrease with increasing  $C_T/\sigma$  because of the decreasing flap collective angles. Half peak-to-peak hinge moment shows virtually no variation

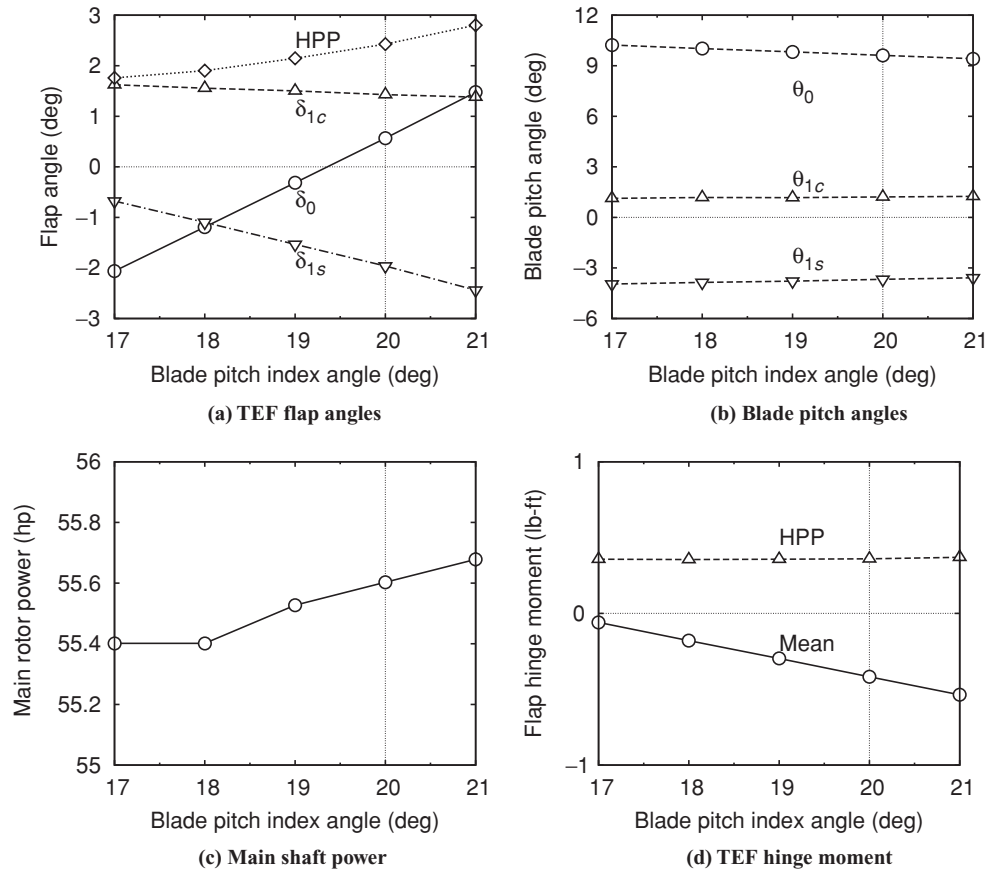


Fig. 6. Effect of pitch index angle on TEF angles, pitch angle, main rotor power, and hinge moments at forward speed of 60 kt ( $\mu = 0.16$ ).

with  $C_T/\sigma$  because of the constant flap cyclic and steady aerodynamic environment in hover.

**Parametric study**

The objective of the parametric study is to evaluate the performance of the teetering rotor of the ultralight helicopter with a plain TEF system for primary control and investigate the effect of various key design variables, namely pitch index angle, flap location and size on rotor performance, and TEF deflections. During the parametric study, only one parameter is changed while others are kept constant. The baseline TEF parameters are listed in Table 3, and the baseline blade pitch index angle is 20°.

Figure 6 illustrates the effect of blade pitch index angle on the flap angle, blade pitch, main rotor power, and flap hinge moment at an advance ratio of 0.16, corresponding to design cruise speed. Figure 6(a) indicates that the flap collective angle,  $\delta_0$ , becomes steadily more algebraically positive, i.e., trailing-edge down, to compensate for the increasing pitch index angle. The magnitude of the flap longitudinal cyclic deflection increases with higher index angle to compensate the blade cyclic pitch produced by the flap collective,  $\delta_0$ , in forward flight. The effect is smaller on lateral flap cyclic than on longitudinal cyclic. The HPP value of the flap deflections increases with the increasing of pitch index angle.

Figure 6(b) illustrates that blade cyclic pitch angles show almost no variations while collective pitch angles show a slight decrease with blade index angle. Figure 6(c) presents the main rotor power and shows an insignificant increase with increasing blade index angles. In Figure 6(d), HPP hinge moments show virtually no variation with blade index angle whereas the mean TEF deflections increase. Figure 6 suggests an optimal blade pitch index angle of 18° for an advance ratio of 0.16 as an overall

consideration of minimizing TEF deflections and main rotor power. In addition, because the required blade pitch angles change with the flight speeds, the optimal pitch index angle also varies with the flight speed. A compromise is required in the selection of an optimal index angle.

Figure 7 examines the effect of TEF location on the TEF deflection and main rotor power at an advance ratio of 0.16. Figure 7(a) shows a reduction in TEF deflections being achieved by moving the flap spanwise location toward the blade tip. The increases in flap effectiveness as it is located toward the blade tip have two contributing factors. First, the dynamic pressure increases toward the blade tip, and second, by moving the point of application of the flap aerodynamic load toward the tip, more of the blade undergoes elastic twist caused by the pitching moment generated by the flap. Figure 7(b) presents the variation of main rotor power with TEF location. The rotor power reaches a minimum at a flap location of 0.75R, although the variation is rather small. The initial decrease in rotor power observed as the flap is moved outboard results from the drag reduction associated with the decreased TEF deflections. As the flap is moved further outboard, this effect is overcome by the effects of increased dynamic pressure and the rotor power increases again. Figure 7 shows an optimum flap location at 0.75R for minimum rotor power and small TEF deflections.

Figure 8 shows that, as may be expected, both TEF collective and cyclic reduce with increasing flap length. Main rotor power presents a minimum with a TEF length of 18%R although again the variation in rotor power is rather small.

The flap chord ratio is a key design parameter because it plays an important role in determining the dominant flap effect, i.e., incremental lift or pitching moment. As shown in Figure 9(a), both flap collective and cyclic deflection are minimized at 25% flap chord ratio, although

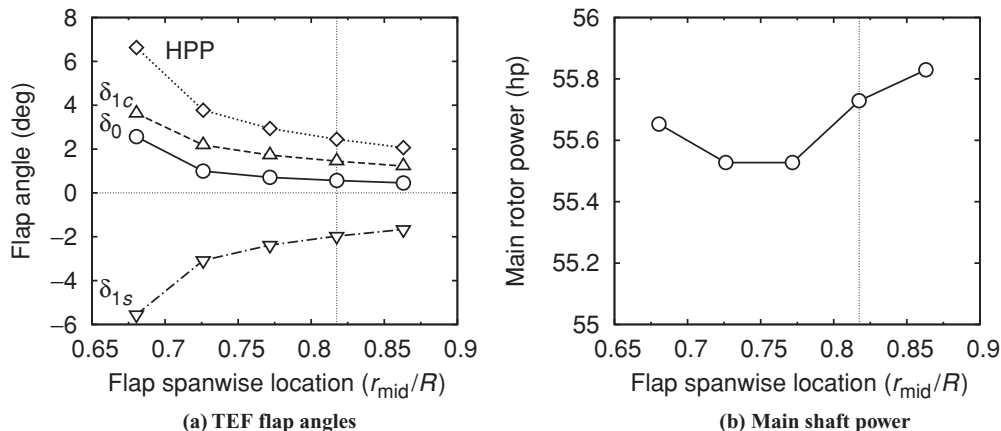


Fig. 7. Effect of TEF location on flap angles and main rotor power at forward speed of 60 kt ( $\mu = 0.16$ ).

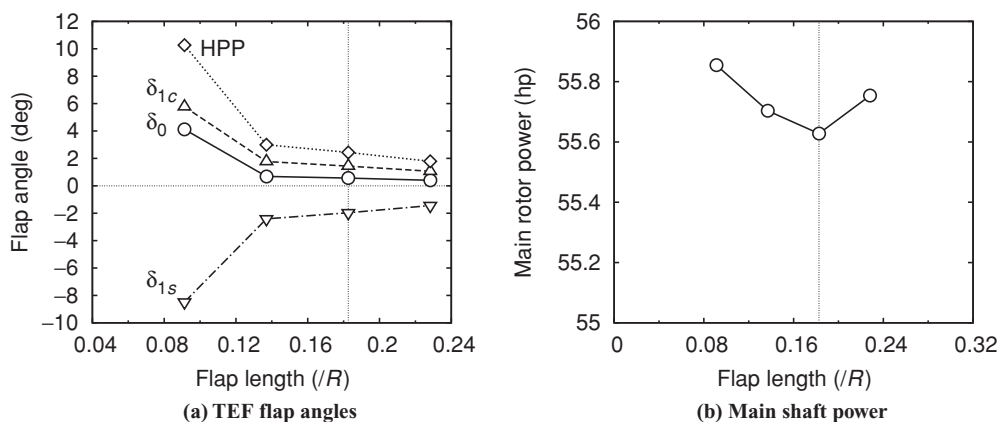


Fig. 8. Effect of TEF length on flap angles and main rotor power at forward speed of 60 kt ( $\mu = 0.16$ ).

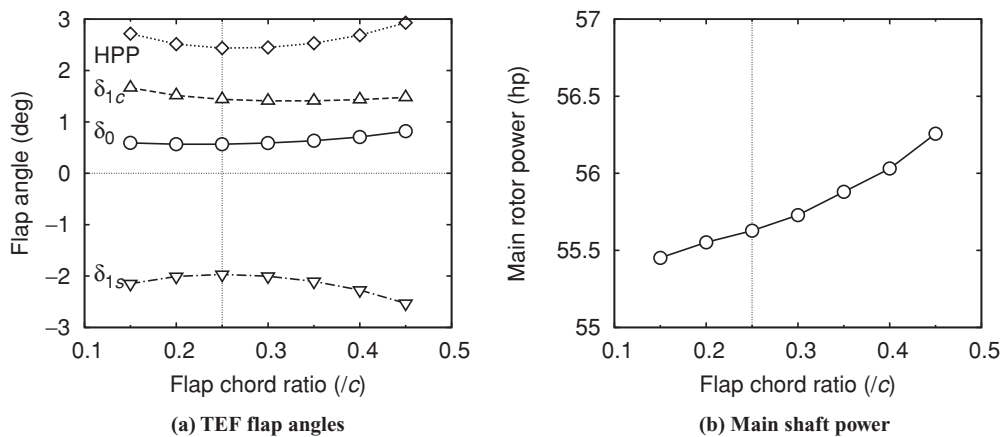


Fig. 9. Effect of TEF chord ratio on flap angles and main rotor power at forward speed of 60 kt ( $\mu = 0.16$ ).

the minimum is rather shallow. Figure 9(b) shows that main rotor power increases with increasing TEF chord ratios. This power increase is especially significant with large flap chord ratios approaching 45%. This is because of the combined effects of increased TEF deflections and the TEF drag associated with a larger flap chord size. Figure 9 suggests an optimum flap chord ratio of 25%.

**Summary and Concluding Remarks**

An ultralight helicopter with TEF for primary control is modeled and the rotor performance and TEF deflections evaluated for a range of

forward speeds. The baseline rotor is a teetering rotor, and the prediction capability of present comprehensive rotorcraft analysis is correlated with the predictions of another comprehensive analysis, CAMRAD II. The correlation is carried out for the baseline rotor without TEF embedded. The predicted blade natural frequencies agree well over a range of rotor speeds except for two higher frequency modes (second inplane and fourth flap bending). The calculated rotor pitch angles, main shaft tilt angles, and blade flapping response are compared at different advance ratios. Rotor pitch angles, longitudinal shaft tilt, and longitudinal flapping angle compare well between two predictions, whereas lateral shaft tilt and lateral flapping angles show some discrepancy. This discrepancy

is attributed to the differences in the inflow models used in the two analyses. Main rotor shaft power compares well between the two analyses at advance ratios above 0.1 but displays some difference at low advance ratios.

The present analysis is then used to evaluate the performance of an ultralight helicopter rotor with TEF as primary flight control and to examine the effects of various key design variables, namely pitch index angle, flap location, and flap geometry on rotor performance and flap deflections. CFD-generated airfoil tables are used to obtain the TEF aerodynamic loads. The following concluding remarks are offered, subject to the limitations of the analysis and the scope of this study:

1) With the design of the baseline TEF system comprising an 18% $R$  plain flap with 25% flap chord ratio located at 82% $R$ , the TEF deflections required to trim the rotor are moderate in the complete range of flight speed; Collective and cyclic flap deflections are both remain below 4°.

2) Compared with a conventional swashplate-controlled rotor, the swashplateless configuration consumes less power in high-speed forward flight. This saving in rotor power results from the reduction of parasite drag through the elimination of the swashplate system. In low-speed flight conditions, the swashplateless rotor consumes slightly less power than the conventional rotor.

3) In hover, the swashplateless rotor consumes slightly less power than the conventional rotor over a wide range of  $C_{TS}$ , corresponding to a slight improvement in figure of merit.

4) Proper selection of pitch index angle, flap location, flap length, and chord ratio is key to minimizing TEF angles, although their effects on rotor power is rather small within the range investigated in this study.

### Acknowledgments

This work was supported by the NASA/Ames under grant NGT252273 with Dr. Chee Tung as technical monitor. We also appreciate useful additional comments from Dr. Matt Floros (ARL/VTD) and the assistance from Mr. Arun Jose (University of Maryland) on using 2D OVERTURNS.

### References

- <sup>1</sup>Pescara, R., "Screw Propeller of Helicopter Flying Machines," US Patent 1,449,129, March 1923.
- <sup>2</sup>Chopra, I., "Status of Application of Smart Structures Technology to Rotorcraft Systems," *Journal of the American Helicopter Society*, Vol. 45, (4), October 2000, pp. 228–252.
- <sup>3</sup>Straub, F. K., "Active Flap Control for Vibration Reduction and Performance Improvement," American Helicopter Society 51st Annual Forum Proceedings, Fort Worth, TX, May 9–11, 1995, pp. 381–392.
- <sup>4</sup>Liu, L., Friedmann, P. P., Kim, I., and Bernstein, D. S., "Rotor Performance Enhancement and Vibration Reduction in Presence of Dynamic Stall Using Actively Controlled Flaps," *Journal of the American Helicopter Society*, Vol. 53, (4), October 2008, pp. 338–350.
- <sup>5</sup>Barrett, R., Frye, P., and Schliesman, M., "Design, Construction and Characterization of a Flightworthy Piezoelectric Solid State Adaptive Rotor," *Smart Materials and Structures*, Vol. 7, (3), June 1998, pp. 422–431.
- <sup>6</sup>Lemnios, A. Z., and Jones, R., "The Servo Flap—An Advanced Rotor Control System," NASA Ames Research Center and American Helicopter Society Vertical Lift Aircraft Design Conference Proceedings, San Francisco, CA, January 17–19, 1990.
- <sup>7</sup>Wei, F.-S., and Jones, R., "Correlation and Analysis for SH-2F 101 Rotor," *Journal of Aircraft*, Vol. 25, (7), July 1988, pp. 647–652.
- <sup>8</sup>Wei, F.-S. J., and Gallagher, F., "Servo-Flap Rotor Performance Flight Testing and Data Identification," American Helicopter Society 57th Annual Forum Proceedings, Washington, DC, May 9–11, 2001, pp. 596–603.
- <sup>9</sup>Straub, F., and Charles, B., "Preliminary Assessment of Advanced Rotor/Control System Concepts (ARCS)," Technical Report 90-D03, USA AVSCOM, August 1990.
- <sup>10</sup>Phillips, N., and Merkley, D., "BHIT's Technical Assessment of Advanced Rotor and Control Concepts," NASA Ames Research Center and American Helicopter Society Vertical Lift Aircraft Design Conference Proceedings, San Francisco, CA, January 17–19, 1990.
- <sup>11</sup>Ormiston, R. A., "Aeroelastic Considerations for Rotorcraft Primary Control with On-Blade Elevons," American Helicopter Society 57th Annual Forum Proceedings, Washington, DC, May 9–11, 2001.
- <sup>12</sup>Shen, J., and Chopra, I., "Swashplateless Helicopter Rotor with Trailing-Edge Flaps," *Journal of Aircraft*, Vol. 41, (2), March–April 2004, pp. 208–214.
- <sup>13</sup>Bir, G., and Chopra, I., "University of Maryland Advanced Rotor Code (UMARC) Theory Manual," Technical Report UM-AERO 94-18, Center for Rotorcraft Education and Research, University of Maryland, College Park, MD, July 1994.
- <sup>14</sup>Shen, J., and Chopra, I., "A Parametric Design Study for a Swashplateless Helicopter Rotor with Trailing-Edge Flaps," *Journal of the American Helicopter Society*, Vol. 49, (1), January 2004, pp. 43–53.
- <sup>15</sup>Yeo, H., and Chopra, I., "Coupled Rotor/Fuselage Vibration Analysis for Teetering Rotor and Test Data Comparison," *Journal of Aircraft*, Vol. 38, (1), January–February 2001, pp. 111–121.
- <sup>16</sup>Shen, J., and Chopra, I., "Aeroelastic Modeling of Trailing-Edge-Flap Helicopter Rotors Including Actuator Dynamics," *Journal of Aircraft*, Vol. 41, (6), November–December 2004, pp. 1465–1472.
- <sup>17</sup>Jose, A. I., Sitaraman, J., and Baeder, J. D., "An Investigation into the Aerodynamics of Trailing Edge Flap and Flap-Tab Airfoils Using CFD and Analytical Methods," American Helicopter Society 63rd Annual Forum Proceedings, Virginia Beach, VA, May 1–3, 2007.
- <sup>18</sup>Johnson, W., "Rotorcraft Aerodynamics Models for a Comprehensive Analysis," American Helicopter Society International 54th Annual Forum Proceedings, Washington, DC, May 20–22, 1998, pp. 71–93.
- <sup>19</sup>Johnson, W., "Rotorcraft Dynamics Models for a Comprehensive Analysis," American Helicopter Society International 54th Annual Forum Proceedings, Washington, DC, May 20–22, 1998, pp. 452–471.
- <sup>20</sup>Dadone, L. U., "US Army Helicopter Design Datcom, Volume 1. Airfoils," Technical Report NASA CR 153247, May 1976.
- <sup>21</sup>Prouty, R. W., *Helicopter Performance, Stability and Control*, Chap. Performance Analysis; Parasite Drag in Forward Flight, PWS Publishers, Boston, MA, 1986.